Front. Phys., 2011, 6(3): 237–250
DOI 10.1007/s11467-011-0164-5

REVIEW ARTICLE

Cavity optomechanics with cold atomic gas

Ke-ye ZHANG (张可烨), **Lu ZHOU** (周鲁), **Guang-jiong DONG** (董光炯), **Wei-ping ZHANG** (张卫平)†

State Key Laboratory of Precision Spectroscopy, Department of Physics, East China Normal University, Shanghai 200062, China

E-mail: †*wpzhang@phy.ecnu.edu.cn*

Received November 26, 2010; accepted December 5, 2010

We present a tutorial review on the topics related to current development in cavity optomechanics, with special emphasis on cavity optomechanical effects with ultracold gases, Bose–Einstein condensates, and spinor Bose–Einstein condensates. Topics including the quantum model and nonlinearity of the cavity optomechanics, the principles of optomechanical cooling, radiation-pressure-induced nonlinear states, the chaotic dynamics in a condensate-mirror-hybrid optomechanical setup, and the spin-mixing dynamics controlled by optical cavities are covered.

Keywords cavity optomechanics, Bose–Einstein condensate, spinor Bose–Einstein condensate, optical bistability

PACS numbers 42.50Pq, 37.30+i, 85.85.+j, 42.65.-k

Contents

1 Introduction

Light interacting with matter can not only be absorbed and emitted by individual atoms but also lead to mechanical effects, as predicted by Maxwell and Bartoli. The radiation pressure force of light was first directly observed in the pioneering experiments of Nichols and Hull and, independently, by Lebedev in 1901 [1, 2]. This force is typically extremely feeble so that the application of this force to manipulate the center-of-mass motion of relatively large mechanical elements is not carried out until 1983. In this year, the group of Walther used an optical cavity to enhance the light intensity resonantly and the radiation pressure force as well [3]. Their setup is the source of the cavity optomechanics where the radiation-pressure-induced back-action of light influences the position of the movable cavity end-mirrors.

At the early stage, as was noted by Braginsky, cavity optomechanics plays a critical role in the design of gravitational-wave detectors [4, 5], such as LIGO and VIGRO, which are composed of enormous Michelson interferometers with movable mirrors [6–8]. Subsequently, the trend turned to exploit micro-mechanical elements with small masses and high-quality mechanical factors, and high-finesse micro-optical cavities to increase the optomechanical effects. Currently, cavity optomechanics is the focus of extensive theoretical and experimental investigations and has witnessed spectacular advances in the latest few years (see Refs. [9, 10] and references therein).

A central paradigm of these researches was the cooling of movable mirror towards the quantum regime, even the quantum mechanical ground state. Rapid progress was made toward this goal using active feedback or intrinsically optical damping in situations ranging from micro- and nano-mechanical systems to large mirrors as used in gravitational wave detectors [11–20]. In quantum regime, cavity optomechanics shows a brilliant and broad perspective of application in quantum information processing [21–23]. Various schemes were proposed for

radiation-pressure-based quantum state engineering [24–26] and for the creation of entangled states of continuous-variable systems [27–30]. Furthermore, the possibility of inducing non-classical behavior in mechanical systems composed of billions of atoms is appealing as a test-bed for fundamental questions in quantum physics [31, 32].

Parallel impressive development was the demonstration of cavity optomechanics effects through other physical objects, e.g., a Cooper-pair box [33], LC circuit [34], a quantum dot [35], and most notably perhaps an ultracold atomic gas [36, 37] or a Bose–Einstein condensate (BEC) [38]. Here the atomic center-of-mass motion dispersively interacting with the cavity field plays the role of the vibrational mode of the mirror driven by the radiation pressure force. Since methods of preparing the atoms in their motional ground state are well developed, using cold atoms in cavity optomechanics allows one to prepare the effective oscillator mode in its quantum ground state. Also, due to the high cooperativity of the cold atomic gas, one reaches the strong-coupling limit of cavity quantum electrodynamics (QED) [39] and high optomechanical coupling rate for mean intracavity photon numbers on the order of unity [38], offering a promising avenue to combine studies of cavity QED and cavity optomechanics.

Besides the atomic external degrees of center-of-mass motion, the role of internal atomic spin degrees of freedom is also explored [40, 41]. The combination of cavity-induced phase shift and the intrinsic spin-exchange interaction of a spinor BEC leads to strong matter-wave and optical bistability, providing a new playground for exploring the spinor dynamics in the frame of cavity optomechanics.

These developments are first steps in opening another frontier broached by optomechanics — the coherent coupling of mechanical elements with atomic systems [42–47] or, more generally, the interfacing of solid-state physics with atomic, molecular, and optical science. It is expected that these developments will lead to basic advances, for instance, in the understanding of the quantum-classical interface [48–50], as well as to applications related to measurement and sensing [51–54] and coherent control [55–57].

The review is organized as follows: In Section 2, we give a brief introduction to the research of conventional cavity optomechanics, including classical nonlinear dynamics, optomechanical cooling of mechanical resonators, and preparing non-classical states through radiation-forces-mediated interactions. In Section 3, we discuss in some detail the effective optomechanical effects realized by an uniform BEC or cold atoms inside a cavity, respectively. In addition, we propose a hybrid system to combine conventional cavity optomechanics and its BEC-based counterpart, where the dynamics of the system is subjected to Hamiltonian chaos in the bistable regime. Section 4 is devoted to a discussion of cavity optomechanics with spinor condensate. Section 5 briefly lists and comments on some further topics, which for various reasons are not covered in the main text.

2 Cavity optomechanics

2.1 Quantum picture of cavity optomechanics

As shown in Fig. 1, in the classical picture of the cavity optomechanics, one consider a Fabry–Pérot cavity with one fixed-end mirror and the other one, of mass m, mounted on a spring or suspended to swing as a pendulum. When this movable mirror is at its equilibrium position $q = 0$, the cavity length is L, and thus the resonance frequency $\omega_n = n\pi c/L (n \in Z)$ where c is the speed of light. An external laser field of frequency ω_p and power $\mathcal{P}_{\rm in}$ is incident on the fixed mirror, generating standing-wave field inside the cavity. The radiation pressure from the standing-wave field pushes the movable mirror against the restoring force. If both the photon absorption by the mirrors and photon-generation process due to the Casimir effect can be ignored, a weak movement of the mirror ($q \ll L$) only results in a shift of cavity resonance frequency with the approximate value $-\omega_n q/L$. However, in the quantum picture, the movement is replaced by the extremely weak deform when the mirror or cantilever is subject to radiation pressure. This deform results in vibrational motion with various mechanical modes.

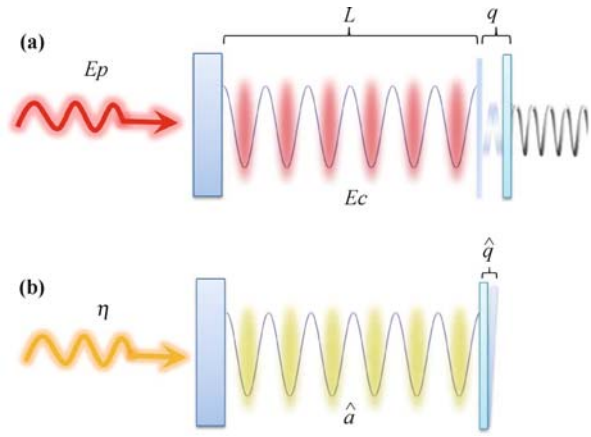

Fig. 1 **(a)** The basic optomechanical setup in classical picture: A cavity consisting of two mirrors, one of which is mounted on a spring. A strong classical light pushes the movable mirror against the restoring force and therefore changes the cavity length. **(b)** In quantum picture, a weak light can only deform the solid structure of a mirror or a cantilever leading to excitation of phonons.

The total Hamiltonian of the system in a frame rotating at the frequency of the laser can be written as [58]

$$\hat{H} = -\hbar\Delta_c \hat{a}^\dagger \hat{a} + \frac{\hbar\omega_m}{2}\left(\hat{p}^2 + \hat{q}^2\right) - \hbar G_0 \hat{a}^\dagger \hat{a}\hat{q}$$

$$-\mathrm{i}\hbar\eta\left(\hat{a}-\hat{a}^{\dagger}\right)+\hat{H}_{\kappa}+\hat{H}_{\gamma} \tag{1}$$

where $\Delta_c=\omega_p-\omega_c$ is the cavity-pump detuning. The intracavity field is described by the annihilation (creation) operator $\hat{a}(\hat{a}^{\dagger})$ and the cavity is locked to the mode with the frequency ω_c. This invoke the condition $|\Delta_c|,\omega_m\ll\Delta\omega_{\mathrm{FSR}}/2$ so that only the single cavity mode is populated by the input laser and the scattering of photons into other modes can be neglected. Here, $\Delta\omega_{\mathrm{FSR}}=\omega_{n+1}-\omega_n=\pi c/L$ is the free spectral range of the cavity. ω_m is the natural frequency of the a mechanical mode of the mirror. This mechanical mode is modeled as an quantum harmonic oscillator with dimensionless momentum operators $\hat{p}$ and position operators $\hat{q}$ satisfying $[\hat{q},\hat{p}]=\mathrm{i}$. m is the effective mass of the oscillator, describing in large part the strength of the coupling between optical and mechanical mode [59]. The third term, as we analyzed above, represents the frequency shift due to the movement of the mirror and is so-called optomechanical term with the coupling rate $G_0=(\omega_c/L)\sqrt{\hbar/(m\omega_m)}$. The term $-\mathrm{i}\hbar\eta\left(\hat{a}-\hat{a}^{\dagger}\right)$ accounts for the external pumping laser where η is related to the input laser power $\mathcal{P}_{\mathrm{in}}$ by $\eta=\sqrt{2\kappa\mathcal{P}_{\mathrm{in}}/(\hbar\omega_p)}$. $\hat{H}_{\kappa}$ and $\hat{H}_{\gamma}$ describe coupling to a bath leading to a cavity damping rate κ and mechanical damping γ, respectively.

The dynamics is determined by the Heisenberg equations and the fluctuation-dissipation processes can be taken into account using the Langevin equations approach. In this case, we can write a set of nonlinear Heisenberg–Langevin equations:

$$\begin{aligned}\partial_t\hat{q}&=\omega_m\hat{p}\\ \partial_t\hat{p}&=-\omega_m\hat{q}-\gamma\hat{p}+G_0\hat{a}^{\dagger}\hat{a}+\hat{\xi}\\ \partial_t\hat{a}&=\left[\mathrm{i}\left(\Delta_c+G_0\hat{q}\right)-\kappa\right]\hat{a}+\eta+\sqrt{2\kappa}\hat{a}_{\mathrm{in}}\end{aligned} \tag{2}$$

where the oscillator is affected by a Brownian stochastic force $\hat{\xi}$ that obeys the correlation function [60, 61]

$$\begin{aligned}\left\langle\hat{\xi}(t)\,\hat{\xi}(t')\right\rangle=\frac{\gamma}{\omega_m}\int\frac{\mathrm{d}\omega}{2\pi}\mathrm{e}^{-\mathrm{i}\omega(t-t')}\\ \cdot\,\omega\coth\left(\frac{\hbar\omega}{2k_{\mathrm{B}}T}+1\right)\end{aligned} \tag{3}$$

where k_{B} is the Boltzmann constant and T is the bath temperature. Remarkably, the quantum Brownian motion is not a Markovian process in general; however, the quantum effects are only achievable by using oscillators with a large mechanical quality factor $\omega_m/\gamma\gg1$. In this limit, $\hat{\xi}$ becomes delta-correlated

$$\left\langle\hat{\xi}(t)\,\hat{\xi}(t')\right\rangle\simeq\gamma\left(2\bar{n}+1\right)\delta(t-t') \tag{4}$$

where $\bar{n}=1/\left[\exp\left(\hbar\omega_m/(k_{\mathrm{B}}T)\right)-1\right]$ is the mean thermal excitation number of the mirror, and the stochastic motion approximates a Markovian process.

The cavity mode decays at the rate κ and is affected by the vacuum radiation input noise $\hat{a}_{\mathrm{in}}$, whose Markovian correlation functions are given by [62]

$$\left\langle\hat{a}_{\mathrm{in}}(t)\,\hat{a}_{\mathrm{in}}^{\dagger}(t')\right\rangle=\left[n(\omega_c)+1\right]\delta(t-t') \tag{5}$$

where $n(\omega_c)$ is the equilibrium mean thermal photon number. Due to the high optical frequency ω_c, this number is insignificant, $n(\omega_c)\simeq0$, even in the room temperature. Besides, we neglect here technical noise sources, such as the amplitude and phase fluctuations of the driving laser.

2.2 Nonlinearity and bistability

Before discussing quantum effects of the optomechanical system, we will briefly review the classical treatment of the equations (2). It is allowed to find analytic solutions for the coupled cavity and mirror dynamics. In particular, one can find the much richer, nonlinear effects. To investigate the purely classical dynamics of the coupled system, we replace the operators by classical variables and neglect various quantum noise, arriving at

$$\begin{aligned}\dot{\alpha}&=\left[\mathrm{i}\left(\Delta_c+G_0q\right)-\kappa\right]\alpha+\eta\\ \ddot{q}+\gamma\dot{q}+\omega_m^2q&=\omega_mG_0\left|\alpha\right|^2\end{aligned} \tag{6}$$

The steady optical intensity $|\alpha_s|^2$ is thus given by a cubic equation

$$\left|\alpha_s\right|^2=\frac{\eta^2}{\kappa^2+\left(\Delta_c+G_0^2\left|\alpha_s\right|^2/\omega_m\right)^2} \tag{7}$$

The solutions to this equation show hysteresis as the pump intensity η^2 [see Fig. 2(a)] or cavity-pump detunning Δ_c [see Fig. 2(b)] increasing, which is precisely analogous to dispersive optical bistability arising from a

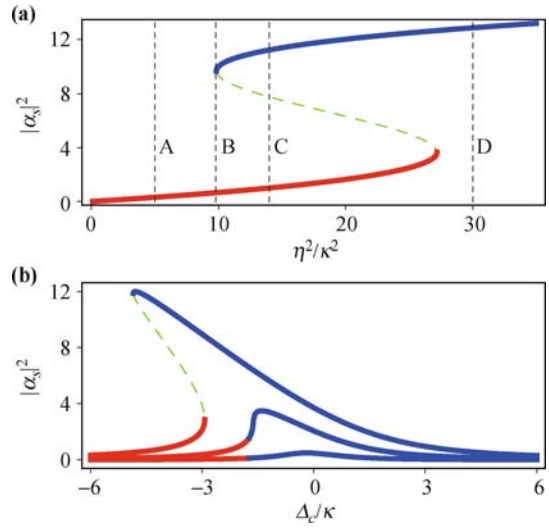

Fig. 2 **(a)** Mean intracavity photon number $|\alpha_s|^2$ of the bistable system versus pump strength for fixed cavity-pump detuning $\Delta_c/\kappa=-4$ and optomechanical coupling rate $G_0^2/(\omega_m\kappa)=0.4$. The green dashed line indicates the instable steady state solutions. **(b)** Mean intracavity intensity versus cavity-pump detuning Δ_c calculated for three different pump strengths $\eta^2/\kappa^2=0.5$, 3.5 and 12.

Kerr medium whose refractive index is intensity-dependent [63].

The dynamics of the coupled mirror-cavity system is governed by two important timescales, the cavity relaxation time $1/(2\kappa)$ and the mechanical oscillation period $1/\omega_m$. This allows to perform an adiabatic approximation in the limit case, which greatly simplifies the analysis of the system's dynamics.

In the good-cavity limit ($\kappa \ll \omega_m$), the intracavity light intensity $|\alpha|^2$ changes slowly such that the position of the mirror adiabatically follows the corresponding change in the radiation pressure. In this case, the mirror impose an intensity-dependent frequency shift $G_0^2 |\alpha|^2 / \omega_m$ on the cavity field.

Conversely, in the bad-cavity limit ($\kappa \gg \omega_m$), the cavity field adiabatically follows the changes in cavity resonance frequency caused by mirror's motion, imposing an position-dependent driving force on the mirror. According to the driving force combining with the inherent restoring force, we can deduce an effective potential [64],

$$V_{\text{eff}} = \frac{\hbar\omega_m}{2} q^2 - \frac{\hbar\eta^2}{\kappa} \arctan \frac{\Delta_c + G_0 q}{\kappa} \tag{8}$$

which provides us with an intuitive picture of the mechanical oscillator dynamics. As shown in Fig. 3(a)–(d), for input intensity below the critical value of the bistable transition, the effective potential always exhibits a single minimum corresponding to the steady solution at the lower branch, but increasing it sees the appearance of a second local minimum indicative of bistability. Further increasing the input intensity past the bistable region the initial minimum disappears as expected. However, in the critical value, the first local minimum of the effective potential degenerates into a plateau; hence, under appropriate circumstances, the mirror subjects to the critical slowing down [65, 66].

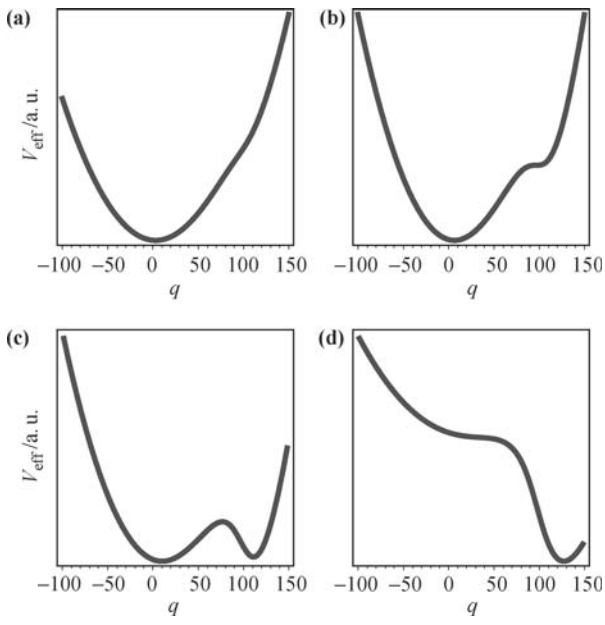

Fig. 3 **(a)–(d)** Show plots of the optomechanical potential V_{eff} for different pumping strengths $\eta^2/\kappa^2 = 5, 9.8, 14$ and 30, corresponding to the dashed upright lines in the steady-state plot Fig. 2(a).

Beyond these two limits, the system's dynamics is complicated and remains mostly unexplored. In particular, at some higher input intensities, the coupled system may enter a state of dissipative chaos [67, 68], where the dynamics is infinitely sensitive to the initial state so that quantitative descriptions are very hard.

2.3 Radiation pressure cooling mechanical mode

Thermal noise is an important limitation to many sensitive measurements such as gravitational wave detection based on cavity optomechanics. Thermally induced deformations of the mirror surface occur as soon as $T > 0$ and constitute the main issue when trying to diminish the noise-induced cantilever motion. In addition to traditional cryogenic techniques that do not allow normally to reach temperatures below $T_c = \hbar\omega_m/(2k_{\text{B}})$, other cooling techniques based on radiation pressure have been proposed. The optomechanical cooling was first theoretically noted by Braginksy [5], who proposed that radiation pressure could be used to "ranquilize" the mechanical mode of an interferometer.

The laser shined upon the mirror leading to radiation pressure force F_{rad}, while in contact with a thermal bath the mirror is also subjected to a Brownian force F_{B}. Thus, it is possible to reduce the motion of the movable mirror by suitably adjusting the radiation pressure force so that $F_{\text{rad}} + F_{\text{B}} \simeq 0$. This is done through the active feedback control [67, 70]: See Fig. 4(a), an intensity and frequency stabilized laser is shined upon the cavity and the motion of the mirror is monitored through homodyne detection of the quadrature of the output field. The resulting signal is fed back to the mirror via a modulation of the laser intensity by an accousto–optic element.

The mirror can also be laser-cooled passively without such feedback, because the radiation pressure force on the mirror is delayed with respect to a sudden change in the mirror's position if the finesse of the cavity is very high. The delayed force can result in a positive optical damping as soon as the laser is red-detuned from the cavity [71]. This principle is easy to understand in the frequency domain. As shown in Fig. 4(b), since the mirror vibrates at frequency ω_m, light reflected off the mirror is scattered in three different frequencies, the original frequency ω_p and two additional sidebands at $\omega_p \pm \omega_m$. If the pump laser frequency slightly red detune from the cavity resonance so that $\omega_p + \omega_m \simeq \omega_c$, the probability of scattering in the $\omega_p + \omega_m$ sideband mode is enhanced as compared to the other two processes, and, therefore, there will be an efficient transfer of energy from the mirror to the light field. Furthermore, when the cavity resonance linewidth κ is smaller than the sideband spacing

$2\hbar\omega_m$, cooling the mirror to its quantum ground state is to be expected [17].

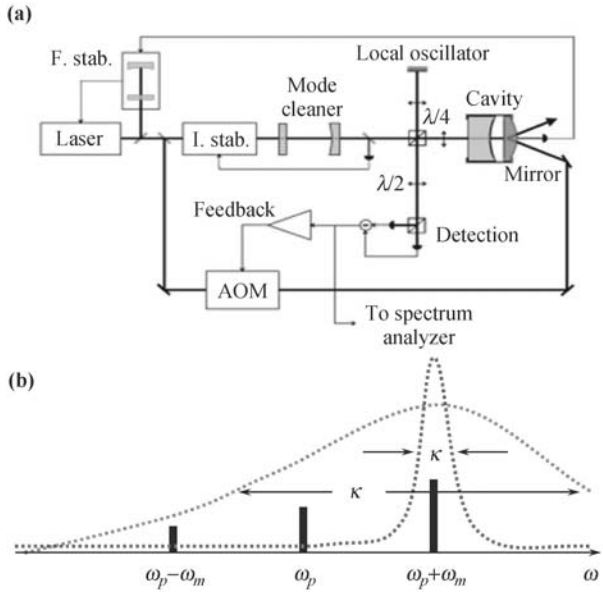

Fig. 4 **(a)** Experimental setup for active feedback cooling of a movable mirror using radiation pressure from a frequency and intensity stabilized laser. The accousto-optic modulator (AOM) modulates the intensity of the laser according the feedback signals. This figure is from Ref. [70]. **(b)** Arrangement of the frequencies in the self-cooling or passive feedback scheme and cavity transmission as a function of frequency. The sideband at $\omega_p + \omega_m$ is resonant so that the scattering in this sideband, corresponding to the annihilation of a mirror phonon, is enhanced. When the cavity linewidth κ is smaller than ω_m, this effect is dominant and named resolved sideband cooling.

2.4 Optomechanical-induced non-classical states

Experimental demonstration of genuine non-classical states of macroscopic mechanical resonators with a mass in the nanogram–milligram range (the mirror or cantilever involve many billions of atoms) is an important step not only for the high-sensitive detection of displacements and forces, but also for the foundations of physics. It would represent, in fact, a remarkable signature of the quantum behavior of a macroscopic object, allowing to shed further light onto the quantum–classical boundary [48–50].

Due to the radiation pressure, the special states of light create superpositions involving macroscopic subsystems so that the quadratures of a light field consisting of many photons could actually become entangled with the positional degree of freedom of a massive oscillator [25, 26]. In order to study how an environment-induced dissipation and decoherence will affect this entanglement, we must study quantum Langevin equations (2), in which thermal noise is taken into account. Since a significant optomechanical entanglement is achieved when radiation pressure coupling is strong, which is realized when the intracavity field is very intense, one can rewrite each Heisenberg operator as a large c-number steady-state value O_s plus an additional small quantum fluctuation $\delta\hat{O}$ with zero mean value and therefore gets the linearized Langevin equations [72]:

$$\begin{aligned}
&\partial_t \delta\hat{q} = \omega_m \delta\hat{p} \\
&\partial_t \delta\hat{p} = -\omega_m \delta\hat{q} - \gamma\delta\hat{p} + G\delta\hat{X} + \hat{\xi} \\
&\partial_t \delta\hat{X} = -\kappa\delta\hat{X} - \Delta\delta\hat{Y} + \sqrt{2\kappa}\hat{X}_{\rm in} \\
&\partial_t \delta\hat{Y} = -\kappa\delta\hat{Y} + \Delta\delta\hat{X} + G\delta\hat{q} + \sqrt{2\kappa}\hat{Y}_{\rm in}
\end{aligned} \tag{9}$$

where $\delta\hat{X} \equiv \left(\delta\hat{a} + \delta\hat{a}^\dagger\right)/\sqrt{2}$ and $\delta\hat{Y} = \left(\delta\hat{a} - \delta\hat{a}^\dagger\right)/(\mathrm{i}\sqrt{2})$ are the cavity field quadratures with corresponding Hermitian input noise operators $\hat{X}_{\rm in}$ and $\hat{Y}_{\rm in}$, respectively. Effective cavity detuning $\Delta = \Delta_c - G_0^2\left|\alpha_s\right|^2/\omega_m$ and optomechanical coupling is enhanced through the effective coupling rate $G = \sqrt{2}G_0\alpha_s$. When the system is stable, the quantum steady state for the fluctuations is a zero-mean bipartite Gaussian state, fully characterized by its 4×4 correlation matrix V [73], with the 2×2 block form

$$V \equiv \begin{pmatrix} A & C \\ C^{\rm T} & B \end{pmatrix} \tag{10}$$

The entanglement between the field quadratures and the mirror vibrational mode is correctly quantified by the logarithmic negativity $E_{\mathcal{N}}$, which in the continuous-variable case can be defined as [74]

$$E_{\mathcal{N}} = \max\left[0, -\ln(2\tilde{d})\right] \tag{11}$$

where $\tilde{d} = 2^{-1/2}\sqrt{\Sigma(V) - \sqrt{\Sigma(V)^2 - 4\det V}}$, with $\Sigma(V) = \det A + \det B - 2\det C$. Therefore, a Gaussian state is entangled if and only if $\tilde{d} < 1/2$, which is equivalent to Simon's necessary and sufficient entanglement criterion [75].

The conditions under which entanglement between several mirrors or membranes can arise is also investigated. In fact, it is possible that, due to the effect of damping, and thermal and quantum noise, the two mechanical modes of the mirrors are never entangled in time, i.e., there is no time instant in which the reduced state of the two mechanical modes is entangled. Entanglement can be instead always present in the frequency domain and quantified by the criterion based on the EPR inequality as [27]

$$\mathcal{E}(\omega) = \frac{\langle\mathcal{R}^2_{q_1-q_2}(\omega)\rangle\langle\mathcal{R}^2_{p_1+p_2}(\omega)\rangle}{\left|\langle[\mathcal{R}_{q_1}(\omega), \mathcal{R}_{p_1}(\omega)]\rangle\right|^2} < 1 \tag{12}$$

where $\mathcal{R}_O(\omega) = [\hat{O}(\omega) + \hat{O}(-\omega)]/2$ is a Hermitian operator and $\hat{O}(\omega) = \tau^{-1/2}\int_{-\tau/2}^{\tau/2} \mathrm{e}^{\mathrm{i}\omega t}\hat{O}(t)\,dt$ is the pseudo Fourier transform for operator $\hat{O}(t)$ in the linearized Langevin equations. Moreover, $\mathcal{E}(\omega)$ goes below 1/4, which indicates the presence of EPR correlations.

Another subject of active research is the development

of squeezing state of nanomechanical systems, which has the potential of reducing the quantum noise arising from vacuum fluctuations of the cantilever and may lead to subshot noise precision measurements. Because of radiation pressure, the cantilever behaves as an effective Kerr medium, leading to a squeezing light in the regions of parameter space close to bistability turning points [76]. An alternative scheme is a three-mirror cavity where the middle movable mirror enables a quadratic optomechanical coupling and therefore subjects to squeezing [77, 78].

3 Cavity optomechanics with cold atomic gas

In the previous section, we discussed conventional cavity optomechanics, wherein optical cooling of a mechanical element or optical nonlinearity, squeezing, and entanglement arise from the coupling between cavity photons and the position of movable mirror. Recently, ultracold atomic gas placed inside optical cavities have been shown to exhibit cavity optomechanical effects. An impressive example is the experiment performed by the group of Esslinger [38]. They utilized collective recoil effect of a uniform BEC to realize a large optomechanical coupling strength with the cavity light field at single-photon level. Cavity optomechanics with ultracold atomic gases was also realized by the group of Stamper–Kurn [36, 37]. In their experiment, lattice-confined cold atoms were shaken by a probe field and the microfabricated atom chip was integrated to obtain a tunable cavity optical nonlinearity and optomechanical frequency shifts. In the following paragraphs, we will give a theoretical explanation of these two experiments in the framework of conventional cavity optomechanics discussed in Section 2. Besides, a novel hybrid system composed both of movable mirror and BEC is discussed. Its dynamics is modeled as the movement of a particle in a singular potential energy surface, which results in a energy-dependent transition from order to chaos.

3.1 Effective–sidemode–mirror approach

This section is devoted to a theoretical interpretation for the analogy that the momentum sidemodes excited by the cavity field act effectively as radiation-pressure-driven oscillators. The scheme is shown in Fig. 5(a): A uniform BEC dispersively interplays with standing-wave optical field inside a micro-cavity. We describe the BEC trapped in the cavity with a simple one-dimensional model in which the atomic motion along the cavity axis is quantized. For large light–atom detunings Δ_a, we can adiabatically eliminate the internal excited state dynamics of the atoms and ignore the effects of spontaneous emission. Considering, in addition, low enough atomic densities that two-body interactions can also be dropped we have

$$\hat{H}_a = \int \hat{\Psi}^\dagger(x)\left(-\frac{\hbar^2}{2m_a}\frac{\mathrm{d}^2}{\mathrm{d}x^2} + \hbar U_0 \hat{a}^\dagger \hat{a}\cos^2 kx\right) \cdot \hat{\Psi}(x)\,\mathrm{d}x \tag{13}$$

where $\hat{\Psi}(x)$ is a bosonic field annihilation operator, m_a is the atomic mass, $U_0 = g_0^2/\Delta_a$ is the dipolar potential depth for a single photon, and k is the wave number of the standing-wave light field. Obviously, the collective density distribution of the BEC is dependent on the dipolar potential, and thus the average photon number $\langle \hat{a}^\dagger \hat{a}\rangle$. If we consider in the following the strong coupling regime $NU_0 \gg \kappa$, where N is the average number of atoms and κ is the cavity damping, the cavity field is also strongly dependent on the collective density distribution of the BEC. More specifically, the dispersive dipolar interaction also impose a BEC-density-dependent frequency shift on cavity mode and therefore change the photon number significantly (but without changing its spatial structure).

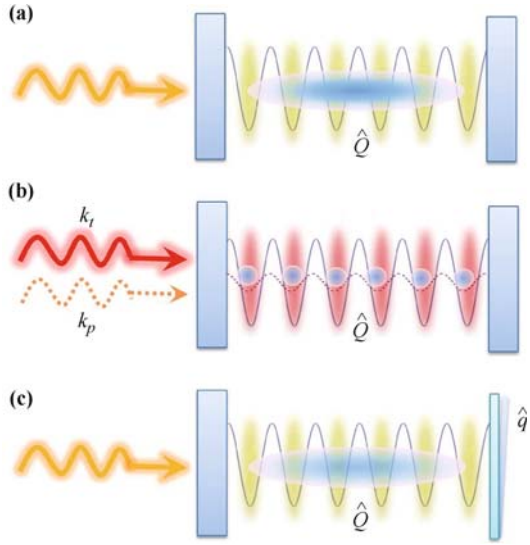

Fig. 5 Schemes for cavity optomechanics with cold atomic gas: **(a)** Coupling a quasi-homogeneous Bose–Einstein condensate dispersively to the standing-wave field inside an optical high-finesse cavity, so that the collective density excitation of condensate acts as the mechanical oscillator driven by the radiation pressure force. **(b)** Non-condensed ultracold atoms are tightly confined within several sites of a static periodic lattice potential generated by the trapping field ω_t, where they perform collective oscillators that strongly couple to the probe field ω_p, and therefore constitute an equivalent optomechanical system. **(c)** One of the cavity's end mirrors is allowed to oscillate, and the others are same as scheme (a). Hence, a cavity, a movable mirror, and a BEC constitute an hybrid optomechanical system.

The photon recoil associated with the absorption and stimulated emission of light by the BEC results in the generation of symmetric momentum side modes at $\pm 2l\hbar k$, where l is an integer. We consider here the simplest situation where the optical field is weak enough that only $l = 1$ side modes are significantly populated. To account for this effect, we then expand the field operator

in Eq. (13) as

$$\hat{\Psi}(x) \simeq \left[\hat{c}_0 + \sqrt{2}\cos(2kx)\hat{c}_2\right]/\sqrt{L} \tag{14}$$

where $\hat{c}_0$ and $\hat{c}_2$ are bosonic annihilation operators for atoms in the zero-momentum state and side-mode components, respectively. With this expansion, H_a simplifies to

$$\hat{H}'_a = \frac{\hbar U_0}{2}\hat{a}^\dagger\hat{a}\left(\hat{c}_0^\dagger\hat{c}_0 + \hat{c}_2^\dagger\hat{c}_2\right) + \frac{\sqrt{2}\hbar U_0}{4}\hat{a}^\dagger\hat{a}\left(\hat{c}_0^\dagger\hat{c}_2 + \hat{c}_2^\dagger\hat{c}_0\right) + 4\hbar\omega_r\hat{c}_2^\dagger\hat{c}_2 \tag{15}$$

where the first and second terms account for the potential energy and the optical coupling between the zero-momentum mode and the side mode of the BEC, respectively. The last term is the energy of the side mode, of frequency $4\omega_r = 2\hbar k^2/m_a$.

In the absence of particle losses, we have $\hat{c}_0^\dagger\hat{c}_0 = N - \hat{c}_2^\dagger\hat{c}_2 \simeq N$, where the approximate equality holds if the zero-momentum component of the condensate is only weakly depleted by the coupling to the momentum side mode. Treating then that component classically via $\hat{c}_0 \to \sqrt{N}$ so that $\hat{H}'_a$ approximately describes a harmonic oscillator mode, which couples via the "displacement" operator $\hat{Q} \equiv (\hat{c}_2^\dagger + \hat{c}_2)/\sqrt{2}$ to the cavity field. If we define an optomechanical coupling rate $G_{\rm sm} = (\omega_c/L)\sqrt{\hbar/(m_{\rm sm}4\omega_r)}$, where $m_{\rm sm} = \hbar\omega_c^2/(L^2NU_0^2\omega_r)$ is the effective mass of the oscillator, $\hat{H}'_a$ reduces into an typical optomechanical form:

$$\hat{H}''_a = \frac{\hbar NU_0}{2}\hat{a}^\dagger\hat{a} + \frac{4\hbar\omega_r}{2}(\hat{P}^2 + \hat{Q}^2) + \hbar G_{\rm sm}\hat{a}^\dagger\hat{a}\hat{Q} \tag{16}$$

where $\hat{P} = \mathrm{i}(\hat{c}_2^\dagger - \hat{c}_2)/\sqrt{2}$ is the "momentum" operator, satisfying the canonical commutation relation $[\hat{Q}, \hat{P}] = \mathrm{i}$. Thus, we can infer about a direct analogy between the coupled condensate-cavity system in the uniform limit and the cavity optomechanical model system introduced in the former section. The role of the mechanical oscillator is played by a collective density oscillation mode of the condensate caused by the population transfer between zero-momentum state and sidemode-momentum states.

3.2 Lattice-confined approach

In this approach, non-condensed ultracold atoms are tightly confined within several sites of a static periodic lattice potential, where they perform collective oscillations that strongly couple to the cavity field. In contrast to the uniform situation, the mechanical oscillation frequency, which is determined by the harmonic potential of the individual sites, can be tuned over a wide range. This provides the opportunity, to approach the resolved sideband regime of cavity optomechanics where retardation effects between the optical and the mechanical dynamics play a dominant role.

Figure 5(b) sketches the geometry of the atom cavity system. A large number of rubidium atoms are distributed over many sites of a one-dimensional intracavity optical lattice formed by a trapping field at wavevector $k_t = 2\pi/850\ \mathrm{nm}^{-1}$, which is different than the probe wavevector $k_p = 2\pi/780\ \mathrm{nm}^{-1}$. A high optical intensity of trapping field leads to a very deep lattice potential, whose each site can be approximated into a harmonic oscillator potential with the trapping frequency $\omega_t = 2\sqrt{s}\omega_r$, where s is the lattice depth scaled by recoil energy E_r. This potential tightly confines each atom at the location of the minimum of the potential, $\bar{q}_i$, plus a deviation from that minimum, δq_i. Due to the large atom-field detuing, the back-action of atoms, that is, the dispersive frequency shift to the trapping field, can be neglected. In contrast, this effect is remarkably for the probe field, and the resulting dispersive frequency shift can be linearly expanded around the position $\bar{q}_i$,

$$\sum_{i=1}^{N} U_0\cos^2(k_p q_i) \simeq U_0 N/2 - \sum_{i=1}^{N} U_0\sin(2k_p\bar{q}_i)\,k_p\delta q_i \tag{17}$$

This motivates to introduce the collective displacement variable

$$Q = \frac{1}{\sqrt{N_{\rm eff}}}\sum_{i=1}^{N} U_0\sin(2k_p\bar{q}_i)\,\delta x_i \tag{18}$$

together with its conjugate momentum

$$P = \frac{1}{\sqrt{N_{\rm eff}}}\sum_{i=1}^{N} U_0\sin(2k_p\bar{q}_i)\,p_i \tag{19}$$

The normalization factor $N_{\rm eff} = \sum_{i=1}^{N}\sin^2(2k_p\bar{q}_i)$ guarantees that the usual commutation relation $\left[\hat{Q}, \hat{P}\right] = \mathrm{i}\hbar$ holds true for the corresponding quantum operators. With these definitions, the Hamiltonian for the atoms can also be written into the same optomechanical form as $\hat{H}''_a$ but with the replacement $4\omega_r \to \omega_m$ and $G_{\rm sm} \to U_0 k_p\sqrt{N_{\rm eff}}$.

3.3 BEC–mirror–hybrid system

In this section, we will consider a model setup consisting of a cavity, a movable mirror, and a BEC inside the cavity [see Fig. 5(c)]. This model was previously discussed in the weak coupling regime $NU_0 \ll \kappa$, the object of that study being the ensuing bistability of the BEC Mott insulator-superfluid transition [46, 66]. In contrast, we now consider a situation where the BEC is strongly coupled to the intracavity field (The main content of this section comes from our publication [47]). At the simplest level, the moving mirror and the condensate side mode can be approximated as two harmonic oscillators coupled by the intracavity optical field, which acts as a nonlinear spring. The coupled quantum Langevin equations of the

system are

$$\begin{aligned}
\partial_t \hat{a} &= \left(\mathrm{i}\tilde{\Delta} + \mathrm{i}G_0\hat{q} - \mathrm{i}G_{\mathrm{sm}}\hat{Q} - \kappa\right)\hat{a} + \eta + \sqrt{2\kappa}\hat{a}_{\mathrm{in}} \\
\partial_t \hat{q} &= \omega_m \hat{p} \\
\partial_t \hat{p} &= -\omega_m \hat{q} + G_0\hat{a}^\dagger\hat{a} - \gamma_m\hat{p} + \hat{\xi} \\
\partial_t \hat{Q} &= 4\omega_r\hat{P} - \gamma_{\mathrm{sm}}\hat{Q} + \hat{f}_Q \\
\partial_t \hat{P} &= -4\omega_r\hat{Q} - G_{\mathrm{sm}}\hat{a}^\dagger\hat{a} - \gamma_{\mathrm{sm}}\hat{P} + \hat{f}_P
\end{aligned} \tag{20}$$

where $\tilde{\Delta} = \Delta_c - NU_0/2$ is the effective detuning and γ_{sm} is the damping of the side-mode mirror with $\hat{f}_Q$ and $\hat{f}_P$ the associated noise operators. We focus in the following on the classical dynamics of the two oscillators by treating their positions and momenta as classical variables. In general, both oscillators and cavity field exhibit a bistable behavior.

In the bad cavity limit, as we discussed in Section 2.2, this bistable behavior can result in rich mirror dynamics. Considering time-scales short enough that their mechanical damping can be ignored, their dynamics is governed by four first-order coupled equations of motion. These equations can be derived from the effective classical Hamiltonian $H_{\mathrm{eff}} = T + V$, with

$$\begin{aligned}
T &= \frac{\hbar\omega_m}{2}p^2 + \frac{4\hbar\omega_r}{2}P^2 \\
V &= \frac{\hbar\omega_m}{2}q^2 + \frac{4\hbar\omega_r}{2}Q^2 \\
&\quad -\frac{\hbar\eta^2}{\kappa}\arctan\left[\left(\tilde{\Delta} + G_0 q - G_{\mathrm{sm}}Q\right)/\kappa\right]
\end{aligned} \tag{21}$$

H_{eff} describes the motion of a particle in the two-dimensional potential $V(q, Q)$, which is generally a double-well potential, as illustrated in Fig. 6. The two local minima A and B correspond to the pairs of bistable values of q and Q at the upper and lower branches, and the saddle-point C corresponds to the unstable values at the dashed branch. The existence of such a saddle point means the Hamiltonian dynamics of the mirrors can undergo a transition to chaos. This chaos originates from the nonintegrable part of the effective Hamiltonian describing the coupled motion of the mirrors — hence, it is called Hamiltonian chaos [79], as opposed to dissipative chaos [67, 68]. The energy-dependent transition from order to chaos is similar to that seen in classic mechanical models, such as the double pendulum and the Hé non–Heiles system [80].

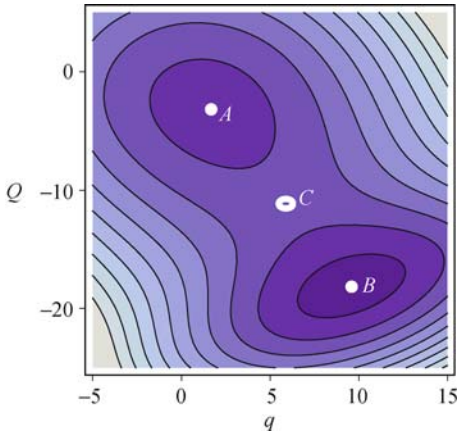

Fig. 6 Two-dimensional contour plot of the effective potential $V(q, Q)$ in a regime where the intracavity optical field, the mirror, and the side-mode excitation all display bistable behavior. A and B are two local minima corresponding to two steady solutions, while C is a saddle point.

To display this transition, we plot Poincaré sections of the four-dimensional phase space at various energy levels. When the energy is very low, the order motion of the particle is characterized by a series of regular elliptic orbits on the Poincaré section (Fig. 7). The situation starts to change when the total energy of the system is close to the saddle-point energy. Some tortuous orbits break into a series of elliptic islands, indicating that the motion is tending to chaos. When the energy is slightly larger than the saddle-point energy, some area of the Poincaré section turn into a "chaotic sea" without any distinctive structure. This area will spread out over the total section as the energy growing up still further. In practice, the chaotic dynamics of the system can be observed by detecting the light transmitted or reflected by the cavity.

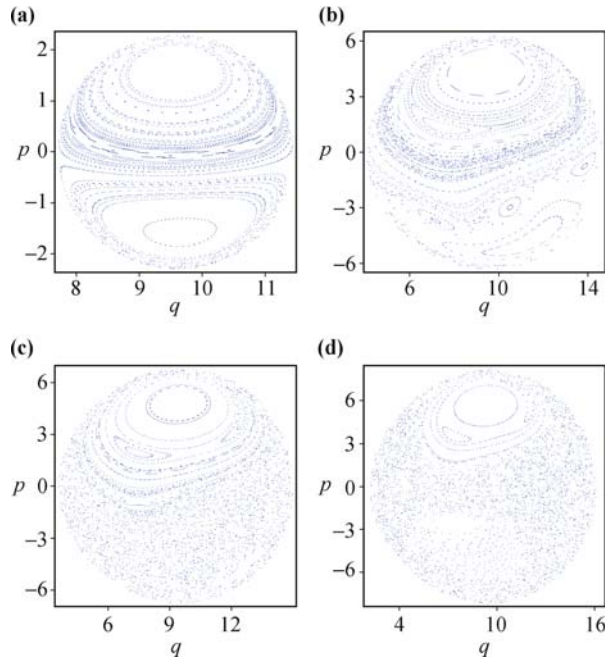

Fig. 7 Poincaré sections (q, p) of the hybrid optomechanical system for **(a)** an energy close to the local minimum energy of point B in Fig. 6, **(b)** an energy near but below the energy of saddle point C, **(c)** an energy slightly above saddle-point energy, and **(d)** an energy significantly above saddle-point energy.

4 Cavity optomechanics with spinor BEC

In the previous section, we discussed cavity optomechanics with scalar BEC, where the interplay between the cavity field and the atomic external degrees of freedom

— the center-of-mass motion of scalar condensates, play a prominent role. This section is devoted to a discussion of cavity optomechanics with spinor BEC, where the cavity field interacts with the atomic internal spin degrees of freedom. Spinor condensate are condensate with hyperfine spin components [81], which becomes accessible by the means of optical dipole trap.

An intriguing property of spinor BEC is that atoms of different spin components can couple to each other via spin-exchange interaction, which give rise to spin mixing [82–84]. The spin mixing dynamics can be described by a nonrigid pendulum. Here, we propose a scheme to exploit the atom–cavity coupling to control the atomic spinor dynamics. Unlike the scalar BEC — standing-wave cavity system discussed in the previous section, the model discussed here cannot be strictly mapped into the cavity optomechanical model. Our interest lies in the nonlinear interaction between the pendulum mechanics of the spinor condensate and the cavity light field. The main content of this section comes from our previous publication [40, 41].

4.1 Model

The model is depicted in Fig. 8. A dilute gas of bosonic atoms with hyperfine spin $F = 1$ are trapped inside the cavity using an optical dipole trap, just as those have been done in Ref. [85] for the single-component condensate. At zero temperature, we assume single-mode approximation (SMA) that atoms in different spin states can be described by the same wave function $\phi(r)$, which is defined by the stationary Gross–Pitaevskii equation; then, each spin component can be associated with an annihilation operator $\hat{c}_i$ ($i = +, -$ and 0). An external weak magnetic field is applied to break the degeneracy and provide the quantization axis. The cavity is designed in the way that only a single mode effectively interacts with the atomic system, which is described by an annihilation operator $\hat{a}$, the cavity mode is π-polarized with its frequency ω_c that couples the atoms in the ground-state manifold to their excited states. The transition selection rule is $\Delta m_{\mathrm{F}} = 0$; however, the transition $|F = 1, m_{\mathrm{F}} = 0\rangle_g \to |F = 1, m_{\mathrm{F}} = 0\rangle_e$ is forbidden. The cavity is driven by a coherent laser field with amplitude η' and frequency ω_p.

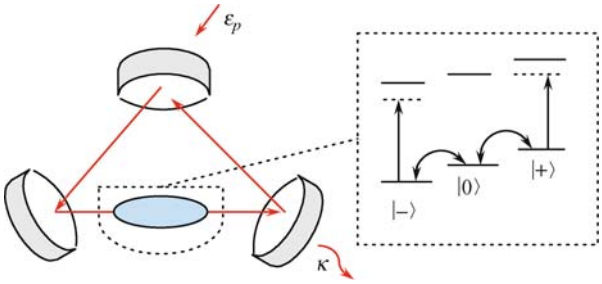

Fig. 8 Schematic diagram showing the system under consideration. An $F = 1$ spinor condensate is trapped inside the cavity using optical dipole trap. The population of different spin components can exchange via spin mixing. The cavity is coherently driven by an external laser with amplitude η and decay with the rate κ. The cavity field is π-polarized and dispersively couple to the atomic system.

The quantum Heisenberg–Langevin equations describing the system read

$$\frac{\mathrm{d}\hat{a}}{\mathrm{d}t} = \left\{\mathrm{i}\left[\delta_c' - U_0'\left(\hat{c}_+^\dagger\hat{c}_+ + \hat{c}_-^\dagger\hat{c}_-\right)\right] - \kappa\right\}\hat{a} + \eta' + \sqrt{2\kappa}\hat{a}_{\mathrm{in}} \tag{22a}$$

$$\mathrm{i}\frac{\mathrm{d}\hat{c}_+}{\mathrm{d}t} = \left(E_+ + U_0'\hat{a}^\dagger\hat{a}\right)\hat{c}_+ + \lambda_a'\left(\hat{c}_+^\dagger\hat{c}_+\hat{c}_+ + \hat{c}_0^\dagger\hat{c}_0\hat{c}_+ - \hat{c}_-^\dagger\hat{c}_-\hat{c}_+ + \hat{c}_-^\dagger\hat{c}_0\hat{c}_0\right) \tag{22b}$$

$$\mathrm{i}\frac{\mathrm{d}\hat{c}_-}{\mathrm{d}t} = \left(E_- + U_0'\hat{a}^\dagger\hat{a}\right)\hat{c}_- + \lambda_a'\left(\hat{c}_-^\dagger\hat{c}_-\hat{c}_- + \hat{c}_0^\dagger\hat{c}_0\hat{c}_- - \hat{c}_+^\dagger\hat{c}_+\hat{c}_- + \hat{c}_+^\dagger\hat{c}_0\hat{c}_0\right) \tag{22c}$$

$$\mathrm{i}\frac{\mathrm{d}\hat{c}_0}{\mathrm{d}t} = E_0\hat{c}_0 + \lambda_a'\left(\hat{c}_+^\dagger\hat{c}_+\hat{c}_0 + \hat{c}_-^\dagger\hat{c}_-\hat{c}_0 + 2\hat{c}_0^\dagger\hat{c}_+\hat{c}_-\right) \tag{22d}$$

where E_i is determined by hyperfine splitting plus the linear and quadratic Zeeman effect. To be more specific, $p' = (E_- - E_+)/2$ and $q' = (E_- + E_+ - 2E_0)/2$ signal the linear and quadratic Zeeman effect, respectively. λ_a' is the anti-symmetric interaction coefficient [82–84], $\delta_c' = \omega_p - \omega_c$ is the cavity-pump detuning. $U_0' = g^2/(\omega_p - \omega_a)$ with g the dipole coupling strength and ω_a the atomic transition frequency. Here, we consider that, in the case of large detuning and weak pump, the atomic upper level can be adiabatically eliminated and the interaction is essentially of dispersive nature. We also assumed that the coupling strength between the cavity field and spin $\pm$ atoms are approximately the same for simplicity. κ is the cavity linewidth.

Here, we should note that, in deriving Eqs. (22), the depletion of the condensate has been neglected. This effect may become important in the long time-scale that the quantum fluctuations of the cavity introduce excess noise to the condensate system [86]. In most realistic cases, cavity decay dominates over the spontaneous decay of atoms, so here we simply assume that, during the time scale we are interested in, the condensate is not significantly depleted, just as those have been done in Refs. [87–90]. A more careful treatment considering the atom loss will be left for further investigation.

4.2 Spin dynamics

The cavity decay rate is typically $\kappa \sim 1$ MHz, while the experimentally measured oscillation frequency of spin population is below 10 Hz for ^{87}Rb [91] and around 50 Hz for ^{23}Na [92]. This means that the cavity field relaxes to the steady state on a much faster timescale than the one on which the spin population evolves. In this limit, the dependence of cavity field on its initial condition is negligible and its dynamics become slave to the

atomic motion, which can then be adiabatically eliminated. Here, we develop a semiclassical description of our system by following the usual mean-field approach. As a first step, we replace the operators $\hat{a}$ and $\hat{c}_i$ with the corresponding $\mathcal{C}$ number $\alpha = \langle \hat{a} \rangle$ and $c_i = \sqrt{N_i} \exp(-i\theta_i)$, where N_i and θ_i represent the number and phase of the bosonic field for the particles in the spin component i, respectively. Next, we change the equations for c_i into the ones for N_i and θ_i and insert in α derived from Eq. (22a). Finally, we take advantage of the existence of two conserved quantities of the system: the total atomic number $N = N_+ + N_- + N_0$ and magnetization $M = N_+ - N_-$, and simplify our problem into the one described by two variables: the normalized population in the spin 0 component $x = N_0/N$ and the relative phase $\theta = 2\theta_0 - \theta_+ - \theta_-$. The equations of motion for x and θ read

$$\frac{\mathrm{d}x}{\mathrm{d}\tau} = 2\lambda_a x \sqrt{(1-x)^2 - m^2} \sin\theta \tag{23a}$$

$$\frac{\mathrm{d}\theta}{\mathrm{d}\tau} = -2\left(q + \frac{U_0 |\alpha|^2}{N}\right) + 2\lambda_a \left[1 - 2x + \frac{(1-x)(1-2x) - m^2}{\sqrt{(1-x)^2 - m^2}} \cos\theta\right] \tag{23b}$$

with

$$|\alpha(x)|^2 = \frac{\eta^2}{1 + [\delta_c - U_0(1-x)]^2} \tag{24}$$

where $m = M/N$, $\tau = \kappa t$ and we have defined the dimensionless parameters

$$\lambda_a = \frac{N\lambda_a'}{\kappa}, \quad q = \frac{q'}{\kappa}, \quad U_0 = \frac{NU_0'}{\kappa}, \quad \eta = \frac{\eta'}{\kappa}, \quad \delta_c = \frac{\delta_c'}{\kappa}$$

From Eq. (23), one can see that the cavity modifies the atomic dynamics in the same manner as the quadratic Zeeman terms q, which will lead to redistribution of atomic population between different spin states through spin mixing. This will in turn shift the cavity resonance frequency and hence modify the intracavity intensity, as can be seen from Eq. (24). Our interest in this model lies in this nonlinear interaction. Following the lines of [89, 90, 93], it is convenient to study the dynamics by constructing the mean-field Hamiltonian H with two conjugate variables x and θ satisfying $\mathrm{d}x/\mathrm{d}\tau = -2\partial H/\partial\theta$, $\mathrm{d}\theta/\mathrm{d}\tau = 2\partial H/\partial x$

$$H = q(1-x) + \lambda_a x \left[1 - x + \sqrt{(1-x)^2 - m^2}\cos\theta\right] + U(x) \tag{25}$$

with $U(x) \equiv \eta^2 \arctan[\delta_c + U_0(1-x)]/N$. The first term of H represents the quadratic Zeeman effect; the second term signals spin-exchange interaction, $U(x)$ is the cavity-induced energy shift.

Before we present the detailed calculation, let us first specify the parameters that will be used. We only consider the anti-ferromagnetic atoms (^{23}Na) with $\lambda_a > 0$ because their spin-mixing effects are relatively large. For sodium atoms with a typical density 2×10^{14} cm^{-3}, $N\lambda_a' \approx 2\pi \times 100$ Hz. We take the cavity decay rate $\kappa = 2\pi \times 100$ kHz, then the value of λ_a is estimated to be 10^{-3}. U_0 is assumed to take the value of -5, $q = 2\lambda_a$ and the total atom number N is taken to be 1000, which is large enough to validate the mean-field treatment.

4.2.1 Equilibrium property

The dynamics of the system can be captured by the contour plot of the mean-field Hamiltonian H, which is intimately related to the fixed points (x_0, θ_0) given by the steady-state solution of Eqs. (23). In the absence of the cavity field, the solutions of the equilibrium equations have been studied in Ref. [94]. Besides the phase-independent solutions of $x = 0$ and $1 - m$ (without loss of generality, we assume $m > 0$) with θ not well-defined, the spinor condensate system support at most one phase-dependent solutions with $\theta = 0$ or π. Here, we make a comparison to see what change was brought by the coupling to the cavity field. The phase diagram identifying different types of solution are mapped out in the parameter space of η^2 (corresponds to the maximum intracavity photon number) and δ_c, as shown in Fig. 9. We can see that the coupling to the cavity will arouse the change of the properties of fixed points. In certain parameter region, the number of different phase-dependent solutions can be more than one; different solution regimes of the coupling system can be crossed by varying δ_c and η^2. Since these two parameters are directly related to the pump laser, this means that the dynamical properties of the system can be easily varied by tuning the pump laser field, which we will illustrate in detail.

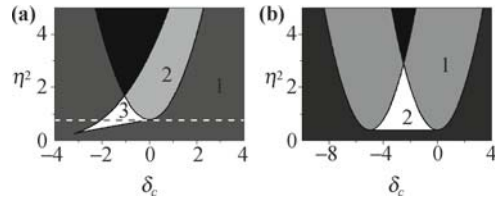

Fig. 9 Phase diagram in the parameter space of δ_c and η^2 for different type of solutions: **(a)** $\theta = 0$; **(b)** $\theta = \pi$. Different regions are differentiated by their colors and are labeled with the numbers of corresponding solutions. The black region means no physical solutions can be found. The parameters are set as $m = 0$, $\lambda_a = 10^{-3}$, $q = 2\lambda_a$, $U_0 = -5$, and $N = 1000$. The red dashed line corresponds to $\eta^2 = 0.8$.

Here, we consider the special case of $m = 0$ and $\theta_0 = 0$; combining the stationary solution of Eq. (23b) with Eq. (24), one can have

$$|\alpha|^2 = \frac{\eta^2}{1 + \left(\Delta + \chi |\alpha|^2\right)^2}$$

where $\Delta = U_0\left(1 + q/2\lambda_a\right)/2 - \delta_c$ and $\chi = U_0^2/(4N\lambda_a)$. It is well known that, when $\eta^2\chi > 8\sqrt{3}/9 \approx 1.54$, the cavity exhibits refractive bistability [95]. Suppose that we fix the intensity of the driving laser field, say that $\eta^2 = 0.8$, which means the maximum intracavity photon number is below unity and we simultaneously have $\eta^2\chi = 5$, so the cavity can display bistable behavior with extremely low photon numbers. By varying the cavity-pump detuning δ_c, the equilibrium properties of the system are changed, as shown in the red dashed line in Fig. 9(a). The corresponding phase-dependent fixed points are derived and their dynamical properties are also studied through the standard linearizion; the results are shown in Fig. 10.

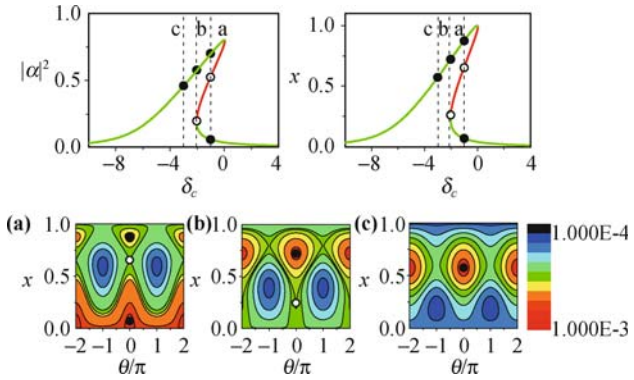

Fig. 10 Mean intracavity photon number $|\alpha|^2$ and the normalized spin population x versus cavity-pump detuning δ_c for the steady-state solutions correspond to the red dashed line in Fig. 9(a) with $\eta^2 = 0.8$. The red line corresponds to dynamically unstable solutions, while the green line means dynamically stable. **(a)**–**(c)** The contour plot of H corresponding to different values of δ_c marked in the upmost figure.

The system exhibits typical bistable behavior in Fig. 10; in certain regions of δ_c near the resonance, it has three stationary solutions, two of which are dynamically stable and the other one is dynamically unstable. Further insights can be achieved by examining the corresponding contour plot of H [Fig. 10(a)–(c)]. Suppose the system is initially prepared in the lower stable branch, as shown in Fig. 10(a), decreasing the cavity-pump detuning δ_c across the resonance renders the system unstable and triggers parametrically excited oscillations, as indicated in Fig. 10(b). Finally, the system will most probably act as a pendulum where the system liberates around the only stable fixed point, as shown in Fig. 10(c). This cavity nonlinear optical phenomenon at low photon numbers has potential applications in optical communication and quantum computation. The underlying physics is that even a single photon can trigger spin exchangement due to the atomic collective strong coupling, and the long-live matter wave coherence built through spin mixing can affect the behavior of subsequent photons interacting with the atom gas. Compared with the bistable behavior observed in Refs. [38, 96], where the motional degrees of freedom of ultracold atomic gases represent the source of coherence affecting light-atom interactions, the unique feature of our system lies in that bistability in the single-photon level are accompanied with bistability of matter waves involving macroscopic number of atoms, as shown in Fig. 10. The matter wave bistability can be directly probed with the nondestructive phase-contrast imaging [97].

4.2.2 Non-equilibrium property

In view that the cavity field can drastically alter the spin-mixing dynamics, here we also consider the non-equilibrium properties of the system. In the absence of the cavity, the population evolution of spinor condensate can be described by a nonrigid pendulum [93, 94, 98–100] and the spin population exhibit periodic oscillations. In the anti-ferromagnetic case, it has been theoretically predicted [93] and experimentally verified [92] that there is a critical magnetic field that corresponds to a critical value of the quadratic Zeeman term q, at which the spin population is trapped in a state with $x = 0$ ($x(\tau \to \infty) = 0$) and the oscillation period diverges. In other words, at the critical value, the system undergoes a transition from the perodic oscillation to the phase-independent solutions.

Now, consider the case with the cavity, assume initially the spinor condensate is prepared in the state (x_i, θ_i), specifically we choose $(x_i = 0.5, \theta_i = 0.5)$ [92]. Consider the case that we fix $\eta^2 = 1$ and vary the cavity-pump detuning δ_c; by propagating the equation of motion Eq. (23), we numerically extract the oscillation period and amplitude, the results are shown in Fig. 11. The oscillation period is typically several tens to hundreds of millisecond, which display a three-peak structure. In order to understand this, the spin population dynamics for

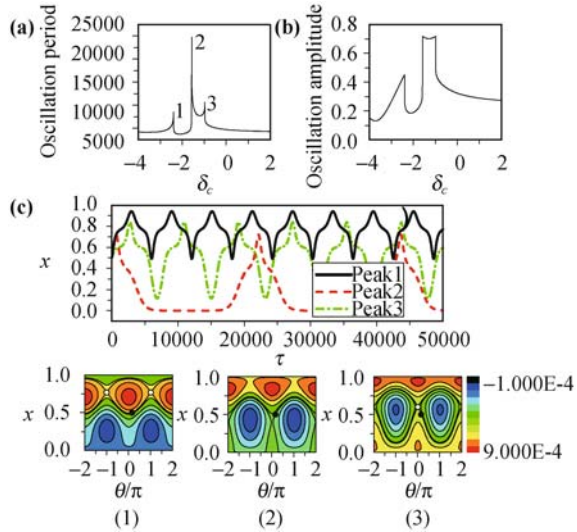

Fig. 11 **(a)** Period and **(b)** amplitude of spin oscillations as a function of cavity-pump detuning δ_c. **(c)** The evolution of x versus τ for the three peaks marked in (a). (1), (2), and (3) The contour plot of H corresponding to the peaks 1, 2, and 3 marked in (a). The black dot refers to the initial state of the system, while the white dots refer to dynamically unstable fixed points.

these three peaks are shown in Fig. 11(c), from which we found out that only for peak 2 the system experiences a transition to phase-independent solution of $x = 0$. The contour plot of H for the three peaks is given in Fig. 11(1)–(3), from which one can understand that the oscillation peaks 1 and 3 are caused by the transition to dynamically unstable fixed points. These transitions will also arouse an abrupt change of the oscillation amplitude, as shown in Fig. 11(b).

5 Future perspectives

Up to now, no experiment has entered into the regime in which the dynamics of a cavity optomechanical system should be described by quantum mechanics, although exciting progresses have been made in this direction. Hence, in the short term, both experimental and theoretical works are mostly devoted to achieve the quantum mechanical ground state of motion.

The study of quantum-to-classical transition provides a number of new issues to cavity optomechanics. An optomechanical setup can exhibit Hamiltonian or dissipative chaotic behavior as discussed in the main text and Ref. [68]. The emergence of chaos in a quantum system reveals many interesting questions [101], and the nonlinear oscillator plays an important role in the analysis of the quantum-to-classical transition of a chaotic oscillator [102]. It might therefore be worthwhile to perform a similar analysis to a chaotic optomechanical system.

Further extensions of the study in the BEC–mirror–hybrid setup could for example involve the entanglement among the atomic motion, quadratures of the cavity field, and the mechanical mode. The realization of such a scheme will open new perspectives for the realization of quantum interfaces and memories for continuous-variable quantum information processing and also for quantum-limited displacement measurements.

Acknowledgements This work was supported by the National Natural Science Foundation of China under Grant Nos. 10588402 (W. Zhang), 10874045 (G. Dong), and 11004057 (L. Zhou), the National Basic Research Program of China (973 Program) under Grant No. 2011CB921604, the Program of Shanghai Subject Chief Scientist under Grant No. 08XD14017, Shanghai Leading Academic Discipline Project under Grant No. B480 (W. Zhang), the "Chen Guang" project supported by Shanghai Municipal Education Commission and Shanghai Education Development Foundation under grant No. 10CG24 (L. Zhou), the Fundamental Research Funds for the Central Universities (L. Zhou, K. Zhang), and the Science and Technology Commission of Shanghai Municipality under Grants Nos. 08PJ1405000 and 07JC14017 (G. Dong).

References

1. E. F. Nichols and G. F. Hull, Phys. Rev. (Series I), 1901, 13: 301
2. P. Lebedev, Annalen der Physik, 1901
3. A. Dorsel, J. D. McCullen, P. Meystre, E. Vignes, and H. Walther, Phys. Rev. Lett., 1983, 51: 1550
4. V. B. Braginsky and A. B. Manukin, Measurement of Weak Forces in Physics Experiments, Chicago: University of Chicago Press, 1977
5. V. B. Braginsky and S. P. Vyatchanin, Phys. Lett. A, 2002, 293, 228
6. R. Drever, G. Ford, J. Hough, I. Kerr, A. Munley, J. Pugh, N. Robertson, and H. Ward, in: Proceedings of the Ninth International Conference on General Relativ-ity and Gravitation, Jena, 14–19 July 1980, Cambridge: Cambridge University Press, 1983: 265
7. A. Abramovici, W. E. Althouse, R. W. P. Drever, et al., Science, 1992, 256: 325
8. C. Bradaschia, R. Del Fabbro, A. Di Virgilio, et al., Nuclear Instruments and Methods in Physics Research A, 1990, 289, 518
9. T. J. Kippenberg and K. J. Vahala, Science, 2008, 321: 1172
10. F. Marquardt and S. M. Girvin, Physics, 2009, 2: 40
11. O. Arcizet, P. F. Cohadon, T. Briant, M. Pinard, and A. Heidmann, Nature (London), 2006, 444: 71
12. S. Gigan, H. R. Böhm, M. Paternostro, F. Blaser, G. Langer, J. B. Hertzberg, K. C. Schwab, D. Baöerle, M. Aspelmeyer, and A. Zeilinger, Nature (London), 2006, 444: 67
13. D. Kleckner and D. Bouwmeester, Nature (London), 2006, 444: 75
14. A. Schliesser, P. Del'Haye, N. Nooshi, K. J. Vahala, and T. J. Kippenberg, Phys. Rev. Lett., 2006, 97: 243905
15. T. Corbitt, C. Wipf, T. Bodiya, D. Ottaway, D. Sigg, N. Smith, S. Whitcomb, and N. Mavalvala, Phys. Rev. Lett., 2007, 99: 160801
16. F. Marquardt, J. P. Chen, A. A. Clerk, and S. M. Girvin, Phys. Rev. Lett., 2007, 99: 093902
17. A. Schliesser, R. Riviére, G. Anetsberger, O. Arcizet, and T. J. Kippenberg, Nat. Phys., 2008, 4: 415
18. J. D. Teufel, J. W. Harlow, C. A. Regal, and K. W. Lehnert, Phys. Rev. Lett., 2008, 101: 197203
19. J. M. Dobrindt, Wilson-Rae, and T. J. Kippenberg, Phys. Rev. Lett., 2008, 101: 263602
20. B. Abbott, R. Abbott, R. Adhikari, et al., New J. Phys., 2009, 11: 073032
21. S. Pirandola, D. Vitali, P. Tombesi, and S. Lloyd, Phys. Rev. Lett., 2006, 97: 150403
22. K. Hammerer, M. Aspelmeyer, E. S. Polzik, and P. Zoller, Phys. Rev. Lett., 2009, 102: 020501
23. A. Geraci and J. Kitching, Phys. Rev. A, 2009, 80: 032317
24. S. Mancini, V. I. Man'ko, and P. Tombesi, Phys. Rev. A, 1997, 55: 3042
25. S. Bose, K. Jacobs, and P. L. Knight, Phys. Rev. A, 1997, 56: 4175
26. W. Marshall, C. Simon, R. Penrose, and D. Bouwmeester, Phys. Rev. Lett., 2003, 91: 130401
27. S. Mancini, V. Giovannetti, D. Vitali, and P. Tombesi, Phys. Rev. Lett., 2002, 88: 120401
28. S. Pirandola, S. Mancini, D. Vitali, and P. Tombesi, Phys. Rev. A, 2003, 68: 062317

29. M. Paternostro, D. Vitali, S. Gigan, M. S. Kim, C. Brukner, J. Eisert, and M. Aspelmeyer, Phys. Rev. Lett., 2007, 99: 250401
30. C. Genes, D. Vitali, and P. Tombesi, Phys. Rev. A, 2008, 77: 050307
31. S. Bose, Phys. Rev. Lett., 2006, 96: 060402
32. J. R. Friedman, V. Patel, W. Chen, S. K. Tolpygo, and J. E. Lukens, Nature (London), 2000, 406: 43
33. A. Naik, O. Buu, M. D. LaHaye, A. D. Armour, A. A. Clerk, M. P. Blencowe, and K. C. Schwab, Nature (London), 2006, 443: 193
34. K. R. Brown, J. Britton, R. J. Epstein, J. Chiaverini, D. Leibfried, and D. J. Wineland, Phys. Rev. Lett., 2006, 97: 133601
35. I. Wilson-Rae, P. Zoller, and A. Imamoglu, Phys. Rev. Lett., 2004, 92: 075507
36. K. W. Murch, K. L. Moore, S. Gupta, and D. M. Stamper-Kurn, Nat. Phys., 2008, 4: 561
37. T. P. Purdy, D. W. C. Brooks, T. Botter, N. Brahms, Z.-Y. Ma, and D. M. Stamper-Kurn, Phys. Rev. Lett., 2010, 105: 133602
38. F. Brennecke, S. Ritter, T. Donner, and T. Esslinger, Science, 2008, 322: 235
39. F. Brennecke, T. Donner, S. Ritter, T. Bourdel, M. Köhl, and T. Esslinger, Nature (London), 2007, 450: 268
40. L. Zhou, H. Pu, H. Y. Ling, and W. Zhang, Phys. Rev. Lett., 2009, 103: 160403
41. L. Zhou, H. Pu, H.-Y. Ling, K. Zhang, and W. Zhang, Phys. Rev. A, 2010, 81: 063641
42. P. Treutlein, D. Hunger, S. Camerer, T. W. Hänsch, and J. Reichel, Phys. Rev. Lett., 2007, 99: 140403
43. D. Hunger, S. Camerer, T. W. Hänsch, D. König, Jörg, P. Kotthaus, J. Reichel, and P. Treutlein, Phys. Rev. Lett., 2010, 104: 143002
44. L. Tian and P. Zoller, Phys. Rev. Lett., 2004, 93: 266403
45. H. Ian, Z. R. Gong, Y. X. Liu, C. P. Sun, and F. Nori, Phys. Rev. A, 2008, 78: 013824
46. W. Chen, K. Zhang, D. S. Goldbaum, M. Bhattacharya, and P. Meystre, Phys. Rev. A, 2009, 80: 011801
47. K. Zhang, W. Chen, M. Bhattacharya, and P. Meystre, Phys. Rev. A, 2010, 81: 013802
48. A. J. Leggett and A. Garg, Phys. Rev. Lett., 1985, 54: 857
49. P. A. M. Neto and D. A. R. Dalvit, Phys. Rev. A, 2000, 62: 042103
50. W. H. Zurek, Rev. Mod. Phys., 2003, 75: 715
51. D. Rugar, R. Budakian, H. J. Mamin, and B. W. Chui, Nature (London), 2004, 430: 329
52. P. Rabl, P. Cappellaro, M. V. G. Dutt, L. Jiang, J. R. Maze, and M. D. Lukin, Phys. Rev. B, 2009, 79: 041302
53. M. D. LaHaye, J. Suh, P. M. Echternach, K. C. Schwab, and M. L. Roukes, Nature (London), 2009, 459: 960
54. M. Bhattacharya, S. Singh, P. Giscard, and P. Meystre, Laser Physics, 2010, 20: 57
55. Y.-J. Wang, M. Eardley, S. Knappe, J. Moreland, L. Hollberg, and J. Kitching, Phys. Rev. Lett., 2006, 97: 227602
56. K. Hammerer, M. Wallquist, C. Genes, M. Ludwig, F. Marquardt, P. Treutlein, P. Zoller, J. Ye, and H. J. Kimble, Phys. Rev. Lett., 2009, 103: 063005
57. S. Singh, M. Bhattacharya, O. Dutta, and P. Meystre, Phys. Rev. Lett., 2008, 101: 263603
58. C. K. Law, Phys. Rev. A, 1995, 51: 2537
59. M. Pinard, Y. Hadjar, and S. Girvin, Eur. Phys. J. D, 1999, 7: 107
60. V. Giovannetti and D. Vitali, Phys. Rev. A, 2001, 63: 023812
61. C. Gardiner and P. Zoller, Quantum Noise, Springer, 2004
62. D. Walls and G. J. Milburn, Quantum Optics, 2nd Ed., Springer, 1995
63. P. Meystre and M. Sargent-III, Elements of Quantum Optics, 4th Ed., Springer, 2007
64. P. Meystre, E. M. Wright, J. D. McCullen, and E. Vi-gnes, J. Opt. Soc. Am. B, 1985, 2: 1830
65. R. Bonifacio and P. Meystre, Opt. Commun., 1979, 29: 131
66. K. Zhang, W. Chen, and P. Meystre, Opt. Commun., 2010, 283: 665
67. T. Carmon, H. Rokhsari, L. Yang, T. J. Kippenberg, and K. J. Vahala, Phys. Rev. Lett., 2005, 94: 223902
68. T. Carmon, M. C. Cross, and K. J. Vahala, Phys. Rev. Lett., 2007, 98: 167203
69. S. Mancini, D. Vitali, and P. Tombesi, Phys. Rev. Lett., 1998, 80: 688
70. P. F. Cohadon, A. Heidmann, and M. Pinard, Phys. Rev. Lett., 1999, 83: 3174
71. T. Kippenberg and K. Vahala, Optics Express, 2007, 15: 17172
72. D. Vitali, S. Gigan, A. Ferreira, H. R. Böhm, P. Tombesi, A. Guerreiro, and V. Vedral, Phys. Rev. Lett., 2007, 98: 030405
73. R. Simon, N. Mukunda, and B. Dutta, Phys. Rev. A, 1994, 49: 1567
74. G. Adesso, A. Sera.ni, and F. Illuminati, Phys. Rev. A, 2004, 70: 022318
75. R. Simon, Phys. Rev. Lett., 2000, 84: 2726
76. C. Fabre, M. Pinard, S. Bourzeix, A. Heidmann, E. Giacobino, and S. Reynaud, Phys. Rev. A, 1994, 49: 1337
77. J. D. Thompson, B. M. Zwickl, A. M. Jayich, F. Marquardt, S. M. Girvin, and J. G. E. Harris, Nature (London), 2008, 452: 72
78. M. Bhattacharya, H. Uys, and P. Meystre, Phys. Rev. A, 2008, 77: 033819
79. R. Hilborn, Chaos and Nonlinear Dynamics: An Introduction for Scientists and Engineers, 2nd Ed., Oxford: Oxford University Press, 2001
80. H. J. Korsch, H. J. Jodl, and T. Hartmann, Chaos, 3rd Ed., Springer, 2008
81. D. M. Stamper-Kurn, M. R. Andrews, A. P. Chikkatur, S. Inouye, H.-J. Miesner, J. Stenger, and W. Ketterle, Phys. Rev. Lett., 1998, 80: 2027
82. T. Ohmi and K. Machida, J. Phys. Soc. Jap., 1998, 67: 1822
83. T.-L. Ho, Phys. Rev. Lett., 1998, 742: 81
84. W. Zhang and D. F. Walls, Phys. Rev. A, 1998, 57: 1248
85. F. Brennecke, T. Donner, S. Ritter, T. Bourdel, M. Köhl, and T. Esslinger, Nature (London), 2007, 450: 268
86. G. Szirmai, D. Nagy, and P. Domokos, Phys. Rev. Lett., 2009, 102: 080401

87. P. Horak, S. M. Barnett, and H. Ritsch, Phys. Rev. A, 2000, 61: 033609
88. P. Horak and H. Ritsch, Phys. Rev. A, 2001, 63: 023603
89. J. M. Zhang, W. M. Liu, and D. L. Zhou, Phys. Rev. A, 2008, 77: 033602
90. J. M. Zhang, W. M. Liu, and D. L. Zhou, Phys. Rev. A, 2008, 78: 043618
91. M.-S. Chang, Q. Qin, W. Zhang, L. You, and M. S. Chapman, Nat. Phys., 2005, 1: 111
92. A. T. Black, E. Gomez, L. D. Turner, S. Jung, and P. D. Lett, Phys. Rev. Lett., 2007, 99: 070403
93. W. Zhang, D. L. Zhou, M.-S. Chang, M. S. Chapman, and L. You, Phys. Rev. A, 2005, 72: 013602
94. D. R. Romano and E. J. V. de Passos, Phys. Rev. A, 2004, 70: 043614
95. R. W. Boyd, Nonlinear Optics, San Diego, CA: Academic Press, 2003
96. S. Gupta, K. L. Moore, K. W. Murch, and D. M. Stamper-Kurn, Phys. Rev. Lett., 2007, 99: 213601
97. J. M. Higbie, L. E. Sadler, S. Inouye, A. P. Chikkatur, S. R. Leslie, K. L. Moore, V. Savalli, and D. M. Stamper-Kurn, Phys. Rev. Lett., 2005, 95: 050401
98. C. K. Law, H. Pu, and N. P. Bigelow, Phys. Rev. Lett., 1998, 81: 5257
99. H. Pu, C. K. Law, S. Raghavan, J. H. Eberly, and N. P. Bigelow, Phys. Rev. A, 1999, 60: 1463
100. H. Pu, S. Raghavan, and N. P. Bigelow, Phys. Rev. A, 2000, 61: 023602
101. S. Habib, K. Jacobs, H. Mabuchi, R. Ryne, K. Shizume, and B. Sundaram., Phys. Rev. Lett., 2002, 88: 040402
102. I. Katz, A. Retzker, R. Straub, and R. Lifshitz, Phys. Rev. Lett., 2007, 99: 040404